Oil Shale, 2026, 43, 1, 31–53 https://doi.org/10.3176/oil.2026.1.02

Reservoir characteristics and influencing factors of multi-lithofacies shales in the Lianggaoshan Formation, Northeast Sichuan Basin

Yuhang Zhou[(a)], Xin Tang[(a)]*, Mian Li[(a,b)]*, Qiuqi Chen[(a)], Zhangping Yan[(a)], Haoran Jiang[(c)], Ruiyu He[(a)], Linyan Li[(a)], Xiaoyi Zhou[(a)]

[(a)] School of Civil Engineering, Chongqing Three Gorges University, Chongqing 404100, China
[(b)] Chongqing Vocational Institute of Safety & Technology, Chongqing 404160, China
[(c)] Chongqing JUNENG Construction (Group) Co., Ltd., Chongqing 401120, China

Received 23 January 2025, accepted 23 January 2026, available online 29 January 2026

Abstract. *This study focuses on the shale of the Lianggaoshan Formation in the Northeast Sichuan Basin, aiming to analyze the pore structure characteristics and influencing factors of its lithofacies – critical for shale oil exploration, as the area has seen major shale oil and gas exploration breakthroughs. Fresh outcrop shale samples were collected in the field, followed by experiments including polarized-light microscope thin-section identification, X-ray diffraction, total organic carbon analysis, gas adsorption, high-pressure mercury intrusion, and scanning electron microscopy. Four lithofacies were classified. Results show the shale contains micropores, mesopores, and macropores; total organic carbon correlates positively with micropore/mesopore parameters but negatively with macropores, while quartz content shows the opposite. The Frenkel–Halsey–Hill fractal dimension correlates positively with total organic carbon, feldspar, and clay minerals, and negatively with quartz. This provides a key theoretical basis for local Lianggaoshan Formation shale oil exploration.*

Keywords: *Northeast Sichuan Lianggaoshan Formation, shale lithofacies, pore structure, TOC, mineral composition.*

1. Introduction

Since the North American shale oil and gas revolution, the global oil and gas resource pattern has undergone major changes. As a major contributor to today's oil and gas resources, shale oil and gas has driven a continuous

* Corresponding author, mikechouzyh@foxmail.com

increase in global demand [1–3]. In recent years, China has steadily increased its shale oil exploitation intensity. China's recoverable shale oil volume grew from 4.37×10^9 tons in 2015 to 1.45×10^{10} tons in 2020, ranking third in the world [4–6]. Compared with North American marine shale reservoirs, most of China's shale reservoirs are formed in lacustrine environments and exhibit a series of unique geological characteristics. The single-layer thickness of China's lacustrine shale reservoirs is relatively thin. The sedimentary environment shows a high degree of complexity, with lithofacies changing rapidly over short distances. Reservoir heterogeneity is extremely prominent [7–9]. This complexity exerts an important restrictive influence on the enrichment of shale oil resources and the enhancement of exploration levels. It also gives rise to a diversity of lithofacies types and intensifies heterogeneity among lithofacies, thereby rendering it difficult to determine pore structure characteristics corresponding to different lithofacies [10, 11]. Consequently, undertaking systematic research on the basis of lithofacies units is of pivotal importance for shale oil exploration and evaluation. Notably, pore structure acts as the core "storage and migration channel" of shale oil – its type, size distribution, and connectivity directly determine the reservoir's oil-bearing capacity and fluid flow efficiency, which are essential prerequisites for accurately evaluating the recoverable potential of shale oil in the Lianggaoshan Formation (Fm).

The evolution of shale pore structure is influenced by a multitude of factors, including total organic carbon (TOC) content, mineral composition, structural deformation, water saturation, and lamina morphology. Zheng et al. [12] proposed that organic matter, along with components such as quartz and clay minerals, significantly impacts the pore structure of the Longmaxi Fm shale in the Sichuan Basin. Cheng et al. [13] indicated that structural deformation leads to the development of additional pores and fractures in shale. Specifically, intergranular pores, interlayer pores, and microfractures among mineral fragments represent the primary contributors to the expansion of the pore structure. Wang et al. [14] exemplified this in the Bossier shale of eastern Texas, USA, and analyzed the characteristics of lamina morphology and pore structure through thin-section petrography.

Previous investigations have predominantly focused on analyzing the pore structure characteristics of black lacustrine shales with high TOC content. However, the sedimentary environment of most lacustrine shale formations is intricate, and lithology changes rapidly. This complexity severely restricts our understanding of shale reservoir characteristics and their formation mechanisms. Hence, elucidating the influencing factors of pore structure across different lithofacies is crucial for exploring the shale reservoir potential of the Lianggaoshan Fm in the Northeast Sichuan Basin [15–17].

Since 2017, China National Petroleum Corporation and China Petroleum & Chemical Corporation have achieved significant new breakthroughs in the shale reservoirs of the Lianggaoshan Fm in the Northeast Sichuan Basis. These achievements indicate that the northeastern Sichuan region is likely to emerge as a crucial new lacustrine shale oil and gas production area in China [18, 19].

The shale strata of the Lianggaoshan Fm exhibit a broad maturity range (Ro: 0.9–1.9%), leading to distinct differences in micropore structures at various stages of maturity evolution [20–22]. To a large extent, the characteristics of the reservoir space in the study area remain unclear, which severely restricts exploration progress.

Consequently, this study focuses on shale samples from the Lianggaoshan Fm in the Northeast Sichuan Basin. Based on lamina characteristics identified through thin-section analysis and results from various geochemical experiments, the lithofacies are classified. By leveraging multiple pore-characterization techniques, such as gas adsorption, high-pressure mercury intrusion, and scanning electron microscopy (SEM), the pore structures of shale reservoirs with different lithofacies are systematically characterized. Moreover, the pore genesis of shale reservoirs in different lithofacies is analyzed, and the key controlling factors of the pore structures across lithofacies are disclosed.

2. Geological survey and experiments

2.1. Geological overview

The research area of this study is situated in the Qilixiang area of the Lianggaoshan Fm within the Northeast Sichuan Basin. This formation is characterized by a series of faults, uplifts, and depressions [23]. Based on geomorphological characteristics, the region can be further classified into the low-and-gentle structural belt in northern Sichuan, the low-and-steep structural belt in western Sichuan, the low-and-steep structural belt in southern Sichuan, and the high-and-steep structural belt in eastern Sichuan [24].

The Lianggaoshan Fm in the Northeast Sichuan Basin predominantly represents delta-lacustrine facies, with a thickness ranging from 1500 to 4000 meters. During the sedimentary period of the Lianggaoshan Fm, a large-scale lake transgression event took place. The internal terrain slope increased, and the surrounding structures rose rapidly [25]. Overall, the formation is mainly composed of semi-deep to deep lake deposits. Additionally, there are some delta deposits in the northwest and east, which supplied clastic materials to the lacustrine facies.

With the successful development of Well Ping'an 1 (yielding a daily output of 112.8 cubic meters), the shale oil of the Lianggaoshan Fm in the Northeast Sichuan Basin achieved a historic breakthrough in 2020. This milestone marks the Sichuan Basin as poised to become the core of China's future shale oil exploration and development [26]. Actual exploration has demonstrated that shale oil production in the study area has reached a historic breakthrough, fully highlighting extensive shale oil resource prospects. This not only contributes to the evaluation of lacustrine shale oil exploration in China but also underscores the strategic significance of this region in the context of national shale oil development [23].

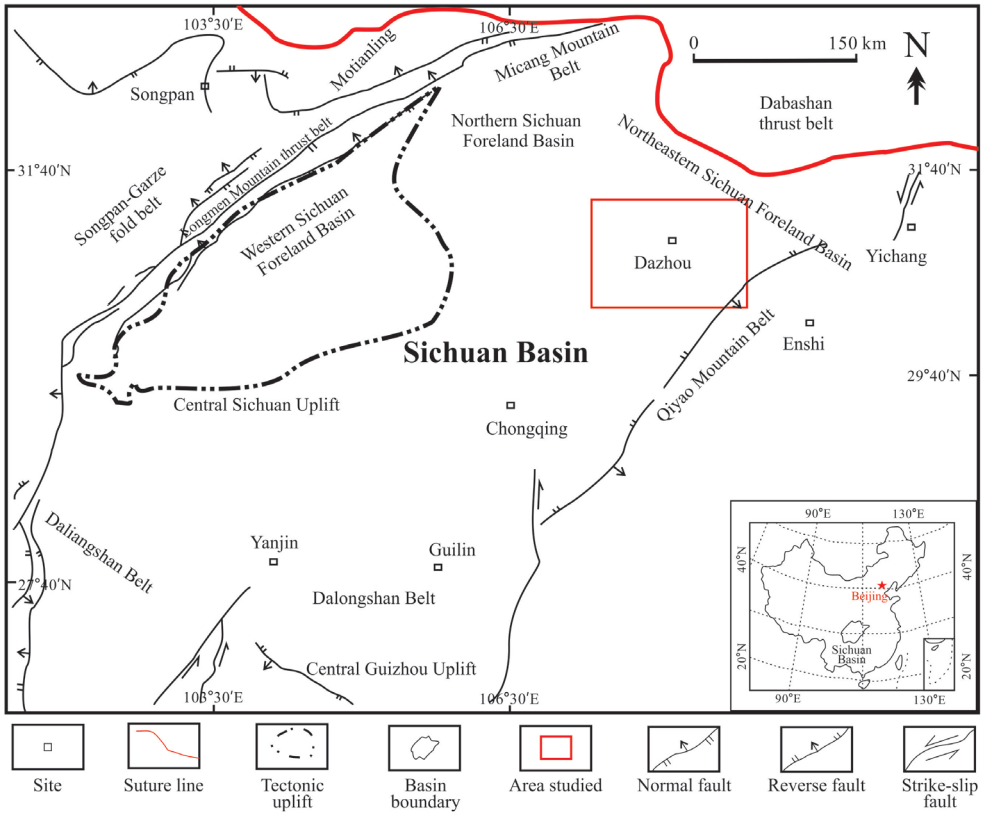

Fig. 1. Geological overview map of the Lianggaoshan Formation study area in the Northeast Sichuan Basin.

2.2. Research methods

A total of 20 fresh outcrop shale samples were collected from the Lianggaoshan Fm in the Northeast Sichuan Basin, and 15 valid samples were selected for subsequent experiments after preliminary screening (excluding samples with obvious weathering, fractures, or impurity contamination to ensure experimental reliability). Rock thin-sections were prepared from the collected samples for identification under a polarized-light microscope. The collected samples were manually ground into powder and sieved to a standard of 80–100 mesh. These powder samples were then utilized for geochemical experiments, including X-ray diffraction (XRD), TOC analysis, carbon dioxide (CO_2) adsorption, and nitrogen adsorption experiments. For the high-pressure mercury intrusion experiment and SEM analysis, block samples measuring 0.5c × 0.5 × 0.5 cm were fabricated.

For thin-section identification under polarized-light microscopy, a Leica DM4 P polarizing microscope was employed. Observation magnifications

of 100× were used for overviews of bedding morphology, while 400× magnification was applied for characterizing mineral/pore details. Five fields of view were selected from each thin section for bedding type classification to ensure representativeness. XRD analysis was performed using a Rigaku Ultima IV diffractometer with a Cu Kα radiation source (λ = 1.5406 Å). The scan range was 5–80° (2θ) with a step size of 0.02° and a scan speed of 5°/min. Mineral content was calculated using the Rietveld refinement method via MDI Jade 6.5 software.

TOC analysis employed a RIKEN CS744 analyzer. Samples underwent 10% hydrochloric acid pretreatment to remove inorganic carbon, followed by analysis at 950 °C in an oxygen flow of 200 mL/min. TOC content was determined by quantifying CO_2 produced from organic carbon combustion. Gas adsorption experiments (CO_2/N_2) employed a JW-BK 132F analyzer. Samples were vacuum-dried at 105 °C for one hour to remove adsorbed water. CO_2 adsorption was conducted at 0 °C (30-second equilibration at each pressure point), while N_2 adsorption occurred at –196 °C (60-second equilibration at each pressure point). Pore parameters were calculated using the Dubinin–Radushkevich (DR) model and Barrett–Joyner–Halenda (BJH) model, respectively.

High-pressure mercury porosimetry was performed using a McMurry AutoPore IV porosimeter (pressure range: 0.001–414 MPa, mercury contact angle: 140°, density: 13.546 g/cm^3). Mercury intrusion/evacuation curves

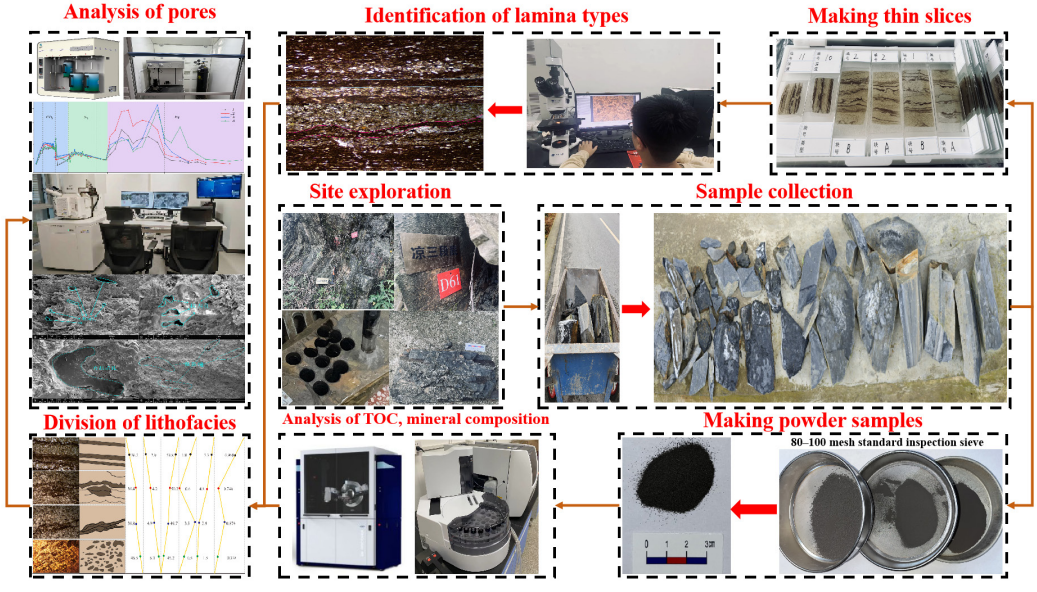

Fig. 2. Experimental workflow for shale samples from the Lianggaoshan Formation.

were automatically recorded to calculate macropore volume. SEM analysis employed a Zeiss Gemini SEM 360 operating in secondary electron mode at 10–20 kV, with a working distance of 8–12 mm and magnification ranging from 500× to 50 000×. Specimens were sputter-coated with a 5 nm gold layer prior to observation to enhance conductivity.

Statistical analysis of experimental data was conducted using Origin 2024 software. Pearson correlation coefficient analysis was applied to evaluate the relationships between TOC/mineral composition and pore-structure parameters (e.g., pore volume, specific surface area), with the coefficient of determination (R^2) indicating fitting quality. For fractal dimension calculation (FHH model), linear fitting of low-temperature nitrogen adsorption data was performed. Each experiment was repeated three times, and the arithmetic mean with standard deviation was reported (relative standard deviation, RSD $< 5\%$) to ensure data reliability.

3. Experimental results

3.1. Classification of shale lithofacies

Through thin-section analysis, and based on the morphology of laminated sedimentary structures, the shale laminations in the study area were classified into three microscopic morphologies: straight, corrugated, and graded types. Straight laminations display continuous development in the form of straight stripes. Corrugated laminations generally present continuous wavy development. Graded laminations bear resemblance to straight laminations; however, the thickness variation between the bright and dark layers is significant, and the change in grain size is prominent. XRD analysis reveals that straight laminations possess the highest clay-mineral content, with corrugated laminations having a slightly lower content, and graded laminations having the lowest. In contrast, the content of quartz and feldspar is highest in graded laminations, followed by corrugated and then straight laminations. In terms of TOC content, straight laminations exhibit the highest values, corrugated laminations have lower values, and graded laminations have the least.

This study integrates the research methodologies proposed by previous scholars [27, 28]. In light of the multi-type lamina characteristics of shale within the Lianggaoshan Fm in the Northeast Sichuan Basin, a lithofacies classification scheme founded on "mineral composition–TOC-lamina morphology" was formulated [29–31]. Among these factors, TOC content serves as a crucial parameter for differentiating lithofacies and can be categorized into four grades: high-carbon (TOC content > 1.5%), medium-carbon (TOC 1.0–1.5%), low-carbon (TOC 0.5–1.0%), and carbon-poor (TOC < 0.5%). Minerals are designated as single-lithology when a single component exceeds 50%, and as mixed-lithology when no dominant component exists (with each component ranging from 25% to 50%).

Table 1. Characteristics of shale lithofacies in the Qilixiang area of the Lianggaoshan Formation, Northeast Sichuan Basin

Lithofacies types	Laminated forms	Average mineral composition, %					Average TOC, %
		Quartz	Feldspar	Clay	Carbonate	Others	
L1 – low-carbon straight-laminated clay shale	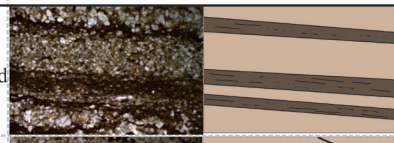	36.2	2.9	53.8	1.8	5.3	0.968
L2 – low-carbon wavy-laminated clay shale	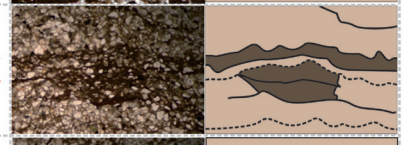	39.4	4.2	50.2	0.6	4.8	0.746
L3 – low-carbon wavy-laminated mixed shale		39.8	4.9	49.7	3.5	2.9	0.874
L4 – carbon-poor graded-laminated mixed shale	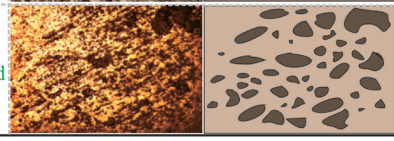	46.5	6.3	45.2	0.5	1.5	0.338

3.2. Pore type characteristics from scanning electron microscopy

For the shale fabrics of different lithofacies types, the differences in pore types and development characteristics were analyzed via SEM observations. The classification of pore types adhered to the previous research scheme [31]. The pores observed under SEM were categorized into intergranular pores, intragranular pores, organic-matter pores, and microfractures [32].

In the study area, samples of lithofacies types L1, L2, and L3 commonly exhibit the distribution of organic matter and clay minerals, with well-developed microstructures. Minerals such as feldspar and flaky mica are distributed along bedding planes, within which intragranular pores have developed. Intergranular and intragranular pores are the most prominently developed pore types. Some intragranular pores have transformed into clay minerals, while others are filled with honeycomb-like illite/smectite mixed layers. The intergranular pores are filled with scaly kaolinite. The sample surfaces are relatively dense. In L4-type samples, organic matter is mainly present in interstitial form, while pyrite is dispersed and locally aggregated (Fig. 3).

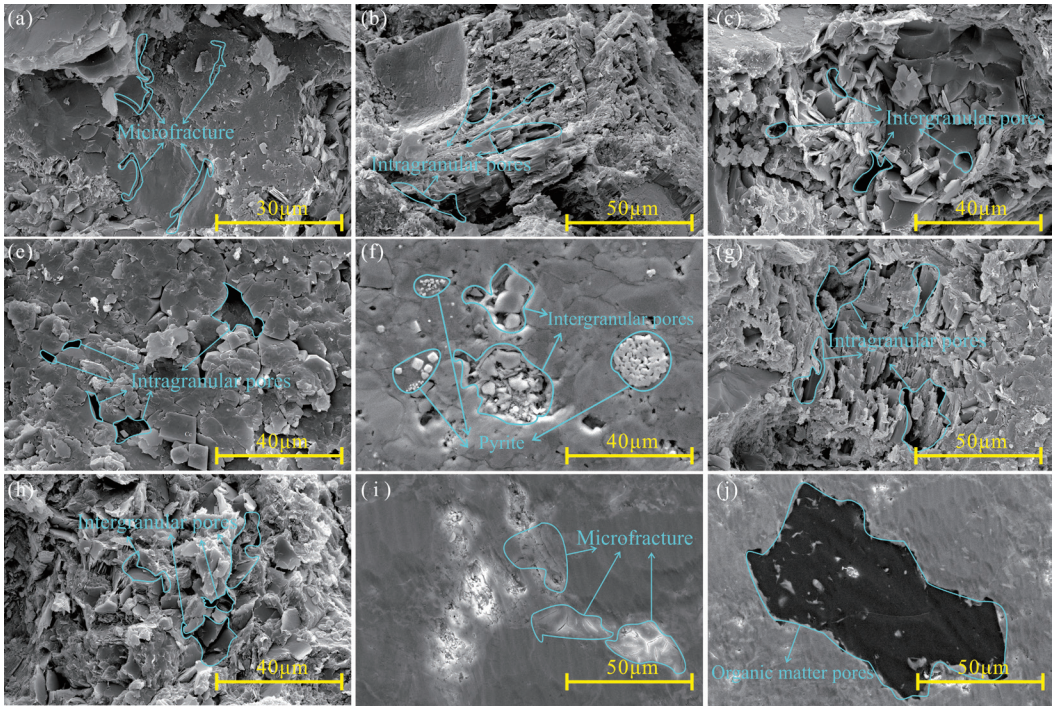

Fig. 3. Shale pore types of the Lianggaoshan Formation, Northeast Sichuan Basin: (a) organic matter associated with clay minerals, with developed micropores; (b) feldspar dissolved along cleavage forming intragranular pores; (c) scale-like kaolinite and a small amount of illite filling intergranular pores, with dense cementation; (d) granular calcite associated with a small amount of illite, with developed intergranular pores; (e) clay minerals developing intergranular pores, partially filled by organic matter, with strawberry-shaped pyrite visible; (f) feldspar dissolved to form intergranular pores, partially transformed into clay minerals; (g) scale-like kaolinite filling intragranular pores, with a small number of intergranular pores developed; (h) clastic minerals dissolved to form intergranular pores, partially transformed into clay minerals, with intercrystalline pores in clay minerals visible; (i) massive organic matter enclosing fine clastic mineral particles, with clay minerals developing a small number of micropores; (j) blocky organic matter developing pores.

3.3. Gas adsorption and high-pressure mercury intrusion experiments

CO_2 adsorption, nitrogen adsorption, and high-pressure mercury intrusion experiments can effectively characterize the pore structure of shale across the entire pore-size range [33]. Based on the IUPAC standards and previous research, pores with diameters of 0–2 nm are classified as micropores, those with diameters of 2–10 nm are classified as mesopores, and pores with diameters greater than 10 nm are classified as macropores [34, 35].

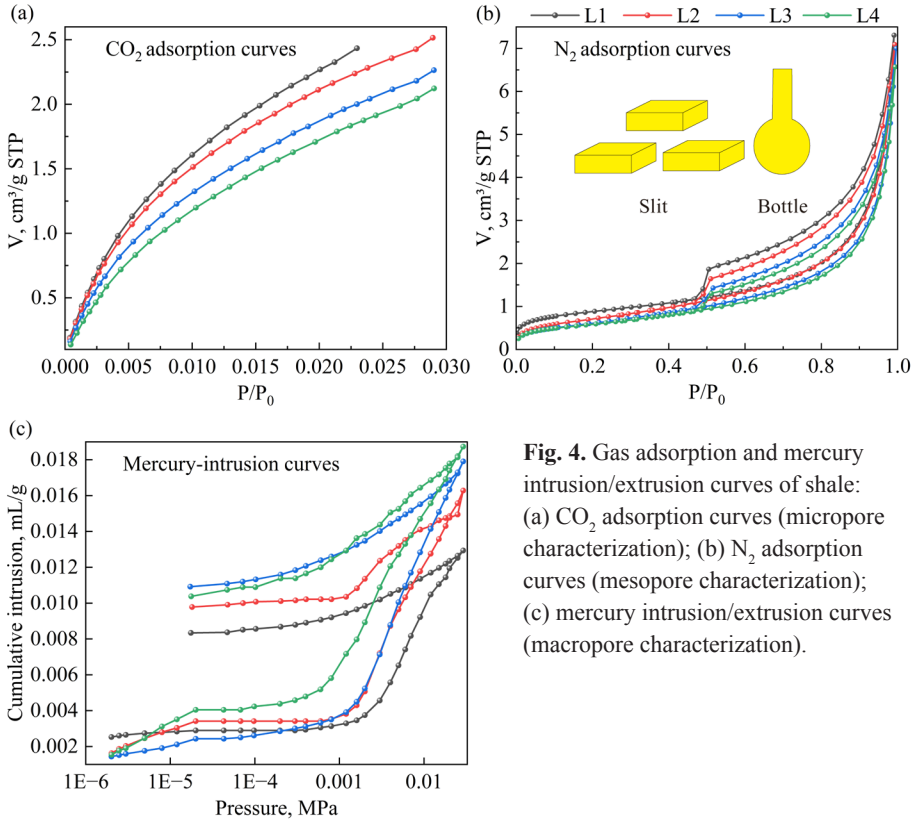

Fig. 4. Gas adsorption and mercury intrusion/extrusion curves of shale: (a) CO_2 adsorption curves (micropore characterization); (b) N_2 adsorption curves (mesopore characterization); (c) mercury intrusion/extrusion curves (macropore characterization).

The shapes of the CO_2 adsorption curves of shale samples remain essentially unchanged, indicating that the micropore morphologies of shale samples of different lithofacies are similar (Fig. 4a). According to the IUPAC classification [34], the nitrogen adsorption curves correspond to type IV, and the hysteresis loops exhibit characteristics of both types H2 and H3, reflecting the presence of slit-shaped and bottle-shaped mesopores (Fig. 4b). For all samples, during the mercury-injection stage of the mercury-intrusion curves, the mercury-injection volume first increases slowly and then rapidly with increasing pressure. During the mercury-withdrawal stage, the decrease in the mercury-withdrawal volume is relatively gentle (Fig. 4c).

The CO_2 adsorption, nitrogen adsorption, and high-pressure mercury intrusion experiments were respectively combined to characterize the pore-size distributions of micropores, mesopores, and macropores in shale samples of different lithofacies. Shale of various lithofacies in the Lianggaoshan Fm shows a certain degree of development of various pore types, mainly concentrated in micropores and macropores. The micropores of shale samples in the Lianggaoshan Fm are primarily in the pore-size range of 0.73–1.22 nm, the mesopores in the range of 2.08–6.27 nm, and the macropores in the range of 11–100 nm (Fig. 5).

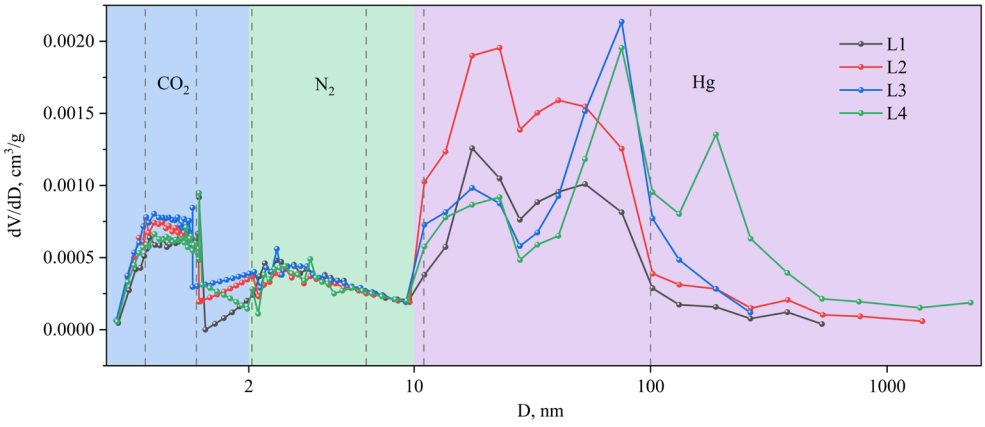

Fig. 5. Pore-size distribution of shale reservoir space in the Lianggaoshan Formation, Northeast Sichuan Basin. Abbreviations: D = pore diameter (nm), dV = differential pore volume (cm^3/g), dD = differential pore diameter interval (nm).

4. Discussion

4.1. Difference mechanism of pore structure in different lithofacies shales

In this study, the pore volume was calculated employing the Barrett–Joyner–Halenda (BJH) model, while the specific surface area was determined by the Brunauer–Emmett–Teller (BET) model. For the shale within the Lianggaoshan Fm, the micropore volume ranges from 0.0044 to 0.0051 cm^3/g, the mesopore volume varies between 0.00227 and 0.00259 cm^3/g, and the macropore volume spans from 0.00818 to 0.00876 cm^3/g. The micropore specific surface area lies between 2.13902 and 2.29159 m^2/g, the mesopore specific surface area ranges from 2.71345 to 2.943879 m^2/g, and the macropore specific surface area is within 1.96937–2.72285 m^2/g. These results indicate that macropores make the most substantial contribution to the overall pore structure (Fig. 6).

This phenomenon can be ascribed to the combined effects of relatively low TOC in this region and the presence of an adequate quantity of brittle minerals (quartz and feldspar, with a combined content exceeding 40%) and clay minerals (content > 50%) [36]. The relatively low TOC content makes it difficult for shale to generate irregular micropores, resulting in a pore structure of low complexity. A certain proportion of brittle minerals helps preserve the integrity of the pore structure and facilitates the formation of intergranular and intercrystalline pores, as well as microfractures within inorganic minerals. This, in turn, is conducive to enhancing the pore connectivity of shale [37].

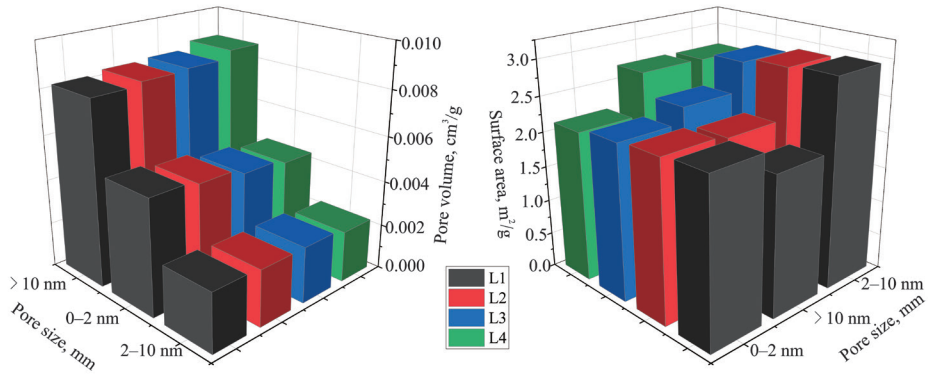

Fig. 6. Distribution map of shale pore volume and specific surface area of the Lianggaoshan Formation, Northeast Sichuan Basin.

In lacustrine shale, the rough surfaces of clay minerals promote the development of additional micropores, exerting a relatively pronounced influence on the micropore structure. Simultaneously, they contribute to maintaining reservoir stability and the optimal functionality of shale [38]. Additionally, carbonate minerals can impact the pore structure of shale [39], presumably because carbonate cements fill pores during the diagenetic process [40].

Based on the experimental results, this study summarizes the mechanisms through which the pore structure is influenced under different lithofacies.

For L1 – low-carbon flat-laminated clay shale, it exhibits the highest TOC and clay-mineral contents, along with the lowest brittle-mineral content, suggesting a relatively high organic-matter content [41]. Micropores and mesopores have a more favorable development potential compared to macropores [42]. Moreover, this lithofacies is more prone to the formation of numerous pores and microfractures, which significantly impact pore volume and specific surface area [43]. This phenomenon exerts a notable influence on the adsorption capacity of oil and gas resources within micropores [44]. Specifically, the quantity of micropores reflects, to a certain degree, the hydrocarbon-generation capacity of shale reservoirs [45].

In contrast, for L4 – carbon-poor graded-laminated mixed shale, its lower clay-mineral content makes it challenging to form micropores and mesopores [46]. As a consequence, the corresponding specific surface area and pore volume are reduced. However, the increase in the volume and specific surface area of macropores improves, to a certain extent, the transport and diffusion of oil and gas resources within shale reservoirs [47].

The distinct pore-structure differences among the four lithofacies (L1–L4) essentially reflect variations in their sedimentary environments and diagenetic processes [48]. For L1 (low-carbon straight-laminated clay shale) and L2

(low-carbon wavy-laminated clay shale), their high clay-mineral and TOC contents are attributed to deposition in a semi-deep to deep lake environment (Section 2.1). This environment featured stable water columns, weak hydrodynamic conditions, and strong reducing conditions – favorable for the preservation of organic matter and the accumulation of fine-grained clay minerals [25, 28]. During early diagenesis, compaction of clay minerals promoted the formation of intercrystalline micropores, while thermal maturation of organic matter (R_o: 0.9–1.9%; Section 1) generated additional organic matter pores, collectively enhancing micropore and mesopore development [20, 35]. In contrast, L4 (carbon-poor graded-laminated mixed shale) was deposited in a delta-front transitional environment, where intermittent hydrodynamic disturbances led to the sorting and accumulation of quartz and feldspar (brittle minerals) [25]. During diagenesis, the low compressibility of brittle minerals prevented the collapse of intergranular spaces, forming macropores dominated by intergranular and dissolution pores (Fig. 3h). Meanwhile, the lack of organic matter (TOC < 0.5%; Table 1) limited the formation of organic micropores, resulting in a macropore-dominated pore structure [32, 40].

4.2. Relationship between shale TOC content, mineral composition, and pore-structure parameters

Based on the preceding mechanism analysis, this section conducts a correlation analysis between TOC content, clay minerals, quartz, and pore-structure parameters. It quantitatively evaluates the relationships between shale lithofacies characteristics and pore-structure parameters, and explores the differential characteristics of pore structures at different scales in shales of various lithofacies.

TOC is positively correlated with the pore volume and specific surface area of micropores and mesopores, and negatively correlated with those of macropores. The pore volume of macropores and the specific surface area of micropores and mesopores are more significantly affected by TOC content. The correlation between the pore volume of micropores and TOC content is slightly stronger than that of mesopores (Fig. 7a, c). This is because organic matter is a significant contributor to micropore development, and TOC content is closely related to the presence of organic matter [49]. During shale reservoir formation, organic matter forms micropores during kerogen pyrolysis and hydrocarbon generation [23]. These processes generate a large number of tiny pores, increasing both pore volume and specific surface area of micropores. Meanwhile, hydrocarbons generated during the maturation of organic matter may cause some micropores to expand into mesopores, and direct mesopore formation within organic matter may also occur, further increasing the pore volume and specific surface area of mesopores [50].

Quartz content is negatively correlated with the pore volume and specific surface area of micropores and mesopores, and positively correlated with those

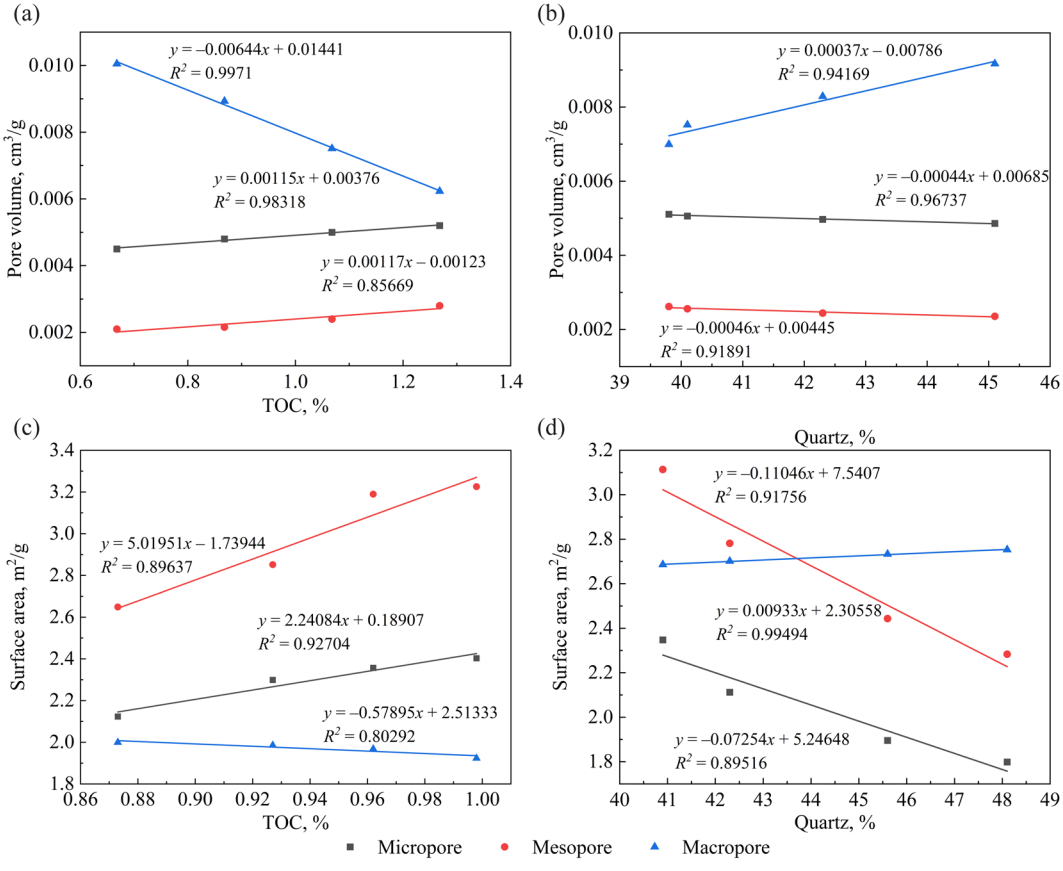

Fig. 7. Correlation analysis between TOC, quartz content, and pore-structure parameters. Left column (a, c): Correlations between TOC content and pore parameters – TOC vs. pore volume (a) and TOC vs. specific surface area (b). Right column (b, d): Correlations between quartz content and pore parameters – quartz content vs. pore volume (b) and quartz content vs. specific surface area (d).

of macropores (Fig. 7b, d). Quartz is relatively compact, and when its content increases, it occupies space, potentially leading to a reduction in the pore volume of micropores and mesopores in shale. Macropores, however, are mainly composed of large intergranular pores, fractures, and some dissolution pores. Therefore, their pore volume is more easily affected by quartz content [24]. The specific surface area of shale pores is mainly contributed by micropores and mesopores. An increase in quartz content dilutes, to a certain extent, the contributions of other minerals with large specific surface areas – such as clay minerals and organic matter – thus reducing the overall specific surface area of the shale [51].

Quartz, being an inert mineral with low chemical activity, rarely undergoes dissolution during diagenesis. Thus, its increase occupies the space originally available for clay minerals and organic matter, reducing micropore and mesopore volume [36]. In contrast, feldspar – a reactive mineral found in L3 and L4 lithofacies – is prone to dissolution under acidic diagenetic fluids generated during organic matter maturation, forming intragranular dissolution pores (Fig. 3b, f) [52]. This explains why L3 (feldspar content: 4.9%; Table 1) has a slightly higher mesopore volume than L2 (feldspar content: 4.2%) – feldspar dissolution partially compensates for the reduction in micropores caused by quartz [40].

4.3. Relationship between TOC content, mineral composition, and fractal dimension of shale

The fractal dimension is an effective method for quantitatively characterizing the microscopic pore structure of shale reservoirs. It can be used to evaluate the complexity and heterogeneity of shale pores. In this paper, the fractal theory is applied to quantitatively characterize the pore-structure features of the Lianggaoshan Fm shale. Based on experimental low-temperature nitrogen adsorption data, the Frenkel–Halsey–Hill (FHH) fractal model was established, and the fractal dimension parameters were calculated using the established model [53, 54]. The formula for the FHH fractal dimension is as follows:

$$\ln V = k \ln\left(\ln\left(\frac{P_0}{P}\right)\right) + C \tag{1}$$

where V represents the gas adsorption volume at adsorption equilibrium pressure (cm^3/g), k is the linear correlation coefficient (a constant related to the adsorption mechanism), and C is a constant (the intercept of the linear fitting curve for the FHH model). In this study, the entire relative-pressure curve was analyzed using the low-temperature nitrogen adsorption data, with capillary condensation as the adsorption mechanism. The fractal dimension D is calculated as follows:

$$D = k + 3 \tag{2}$$

In this research, a quantitative analysis was conducted to examine the relationships among TOC content, mineral components, and fractal dimension. The objective was to explore differences in pore structures across diverse shale lithofacies and to assess the impacts exerted by TOC content and mineral components shale pore characteristics.

The calculated fractal dimension (D) of the Lianggaoshan Fm shale spans from 2.51123 to 2.53098, while the coefficient of determination (R^2) ranges between 0.97061 and 0.98639. These values indicate a relatively high degree of fitting (Fig. 8).

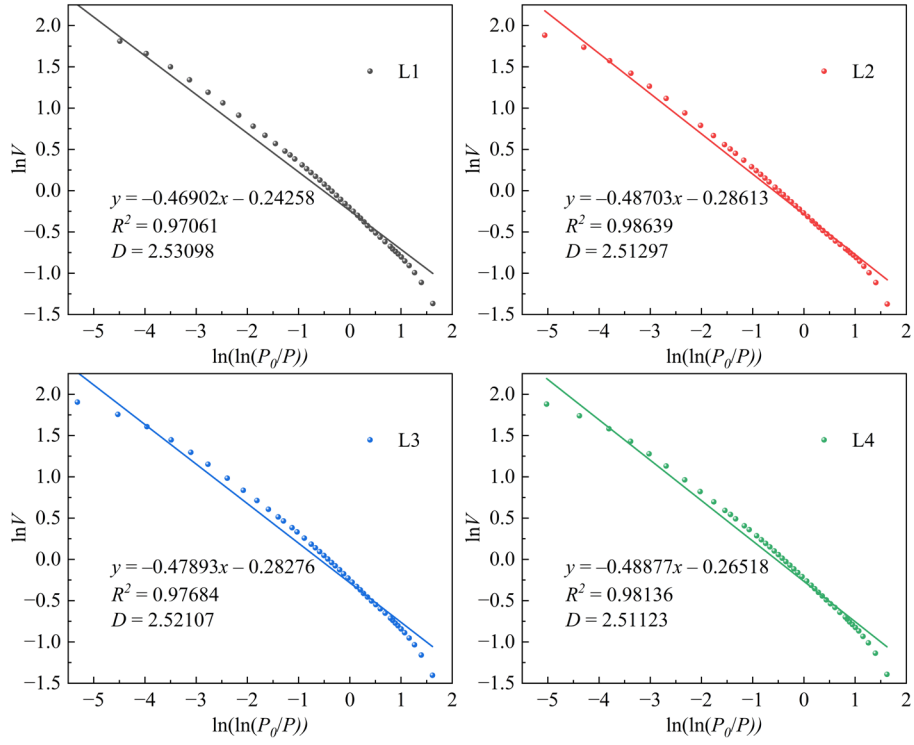

Fig. 8. Fractal fitting curves of shale samples with different lithofacies in the Lianggaoshan Formation, Northeast Sichuan Basin.

A positive correlation exists between the fractal dimension and TOC content. Specifically, as TOC content increases, the fractal dimension becomes larger, signifying a more intricate pore structure (Fig. 9). Because micropores are predominantly developed within organic matter, a lower TOC content corresponds to a smaller fractal dimension, leading to a simpler pore structure [55].

Conversely, a negative correlation is observed between the fractal dimension and quartz content. Owing to the stable crystal structure of quartz, it presents a relatively regular and less complex pore structure. Hence, an increase in quartz content results in a decrease in the fractal dimension [12].

The fractal dimension is positively correlated with feldspar content. This is attributed to the fact that feldspar dissolution generates secondary pores, augmenting the overall complexity of the shale pore structure [52].

Moreover, the fractal dimension also demonstrates a positive correlation with clay-mineral content. This can be explained by the large specific surface area of clay minerals, within which micropores and mesopores are predominantly distributed, thereby contributing to a high level of pore complexity [55].

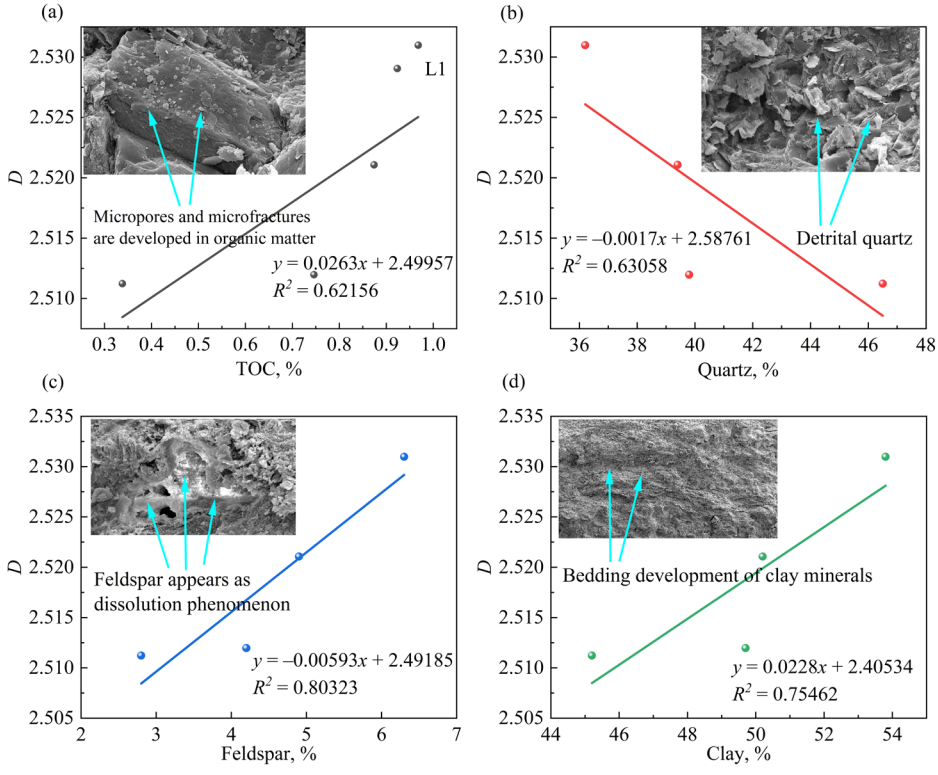

Fig. 9. Correlation analysis between the fractal dimension of Lianggaoshan Formation shale and TOC, quartz, feldspar, and clay-mineral contents.

4.4. Relationship between pore characteristics and shale reservoir potential

The pore-structure parameters (volume, specific surface area, and connectivity) of the Lianggaoshan Fm shale directly determine their shale oil reservoir potential, as verified by experimental data. Micropores and mesopores serve as the primary carriers for adsorbed shale oil, whereas macropores facilitate the storage of free oil [32, 52]. The L1 facies exhibits the largest micropore volume (0.0051 cm^3/g) and the highest mesopore specific surface area (2.94 m^2/g), endowing it with strong adsorption capacity. This is further supported by its TOC content (0.968%), as organic pores can absorb two to three times more oil than inorganic pores [12, 50].

Macropores (diameter > 10 nm) and microfractures serve as key flow pathways for shale oil [37]. Facies L4 exhibits the largest macropore volume (0.00876 cm^3/g) and the highest brittle-mineral content (quartz + feldspar = 52.8%; Table 1), indicating superior pore connectivity.

Within the study area, facies L1–L3 – characterized by well-developed micropores and mesopores with strong oil-trapping capacity – are suitable as oil-rich reservoirs, whereas facies L4, dominated by macroporosity with good fluid mobility, can serve as oil migration pathways. This reservoir–channel coupling provides a geological basis for selecting favorable exploration sections in the Lianggaoshan Fm of Northeast Sichuan [19, 23].

This study advances lacustrine shale reservoir research in three key aspects. First, unlike previous studies focused on high-TOC marine shales (e.g., Longmaxi Formation, Barnett Shale), this work systematically characterizes the pore structure of low-TOC lacustrine shales (TOC: 0.338–0.968%) in the Lianggaoshan Fm. The findings demonstrate that even low-TOC lacustrine shales can form effective reservoirs via clay interstitial pores and brittle-mineral macropores, thereby supplementing understanding of lacustrine shale reservoir genesis mechanisms [10, 24]. Second, by establishing an lithological facies–pore structure–reservoir potential correlation model (Figs 6, 7, 9), this study provides a quantitative method for evaluating low-TOC lacustrine shale reservoirs, improving upon the qualitative facies classifications of earlier studies [29, 31]. Third, the findings clarify the influence of sedimentary environments (semi-deep lake and deltaic foreland) on pore development in the Lianggaoshan Fm, providing a reference for predicting pore structures in analogous global lacustrine shale sequences (e.g., Denver Basin, Wakamulta Fm).

5. Conclusions

Through a series of physical experiments and in-depth data analyses, this study meticulously investigated the microscopic structural characteristics of shale in the Lianggaoshan Formation. Lithofacies classification was accomplished by comprehensively integrating the outcomes of thin-section analysis, X-ray diffraction experiments, and TOC content measurements. Pore and fracture features were examined microscopically using scanning electron microscopy. Quantitative characterization of shale microstructures was conducted through carbon dioxide adsorption, nitrogen adsorption, and high-pressure mercury intrusion experiments. Based on nitrogen adsorption data, the fractal dimension was calculated to explore the pore-structure features of the Lianggaoshan Formation shale. Drawing on experimental results and subsequent analyses, the following conclusions were reached:

1. The laminated shale of the Lianggaoshan Formation can be taxonomically divided into four distinct lithofacies: L1 – low-carbon straight-laminated clay shale, L2 – low-carbon wavy-laminated clay shale, L3 – low-carbon wavy-laminated mixed shale, and L4 – carbon-poor graded-laminated mixed shale. L1 shale exhibits the highest average TOC and clay-mineral contents, whereas L4 shale contains the greatest quartz and feldspar content. Organic matter and clay minerals are widely distributed in L1–L3 samples, where microfractures are well developed.

2. In the Lianggaoshan Formation shale, the micropore volume ranges from 0.0044 to 0.0051 cm^3/g, the mesopore volume from 0.00227 to 0.00259 cm^3/g, and the macropore volume from 0.00818 to 0.00876 cm^3/g. The specific surface area of micropores extends from 2.13902 to 2.29159 m^2/g, that of mesopores varies from 2.71345 to 2.943879 m^2/g, and that of macropores ranges from 1.96937 to 2.72285 m^2/g. TOC content and mineral composition exert a profound influence on shale pore structure. TOC is positively correlated with the pore volume and specific surface area of micropores and mesopores but negatively correlated with those of macropores. Quartz content exhibits a negative correlation with the pore volume and specific surface area of micropores and mesopores, while demonstrating a positive correlation with those of macropores.
3. The fractal dimension (D) of the Lianggaoshan Formation shale ranges from 2.51123 to 2.53098, and the coefficient of determination (R^2) ranges from 0.97061 to 0.98639, signifying a relatively high degree of fitting. The fractal dimension is positively correlated with TOC content – lower TOC content corresponds to a simpler pore structure. Quartz, with its relatively regular and less complex pore structure, exhibits a negative correlation with the fractal dimension. Feldspar dissolution enhances the complexity of the shale pore structure, thereby presenting a positive correlation with the fractal dimension. Clay-mineral content, characterized by high pore complexity, is also positively correlated with the fractal dimension.

Data availability statement

All data used in this article are publicly available. No new data were created or analyzed in this study.

Acknowledgments

This research was supported by the Chongqing Natural Science Foundation of China (project No. CSTB2022NSCQ-MSX0333) and the Science and Technology Research Program of the Chongqing Municipal Education Commission (projects Nos KJZD-K202401205 and KJQN202401214). The publication costs of this article were partially covered by the Estonian Academy of Sciences.

References

1. Sun, S., Liang, S., Liu, Y., Liu, D., Gao, M., Tian, Y. et al. A review on shale oil and gas characteristics and molecular dynamics simulation for the fluid behavior in shale pore. *Journal of Molecular Liquids*, 2023, **376**, 121507. https://doi.org/10.1016/j.molliq.2023.121507
2. Lv, J., Jiang, F., Hu, T., Zhang, C., Huang, R., Hu, M. et al. Control of complex lithofacies on the shale oil potential in ancient alkaline lacustrine basins: the Fengcheng Formation, Mahu Sag, Junggar basin. *Geoenergy Science and Engineering*, 2023, **224**, 211501. https://doi.org/10.1016/j.geoen.2023.211501
3. Chen, H., Fang, D., Gu, H., Huang, W. Comprehensive evaluation of shale reservoir reconstruction based on microseismic and multidisciplinary integration. *Adsorption Science & Technology*, 2022, 5095254. https://doi.org/10.1155/2022/5095254
4. Cheng, G., Wu, C., Jiang, B., Li, F., Li, M., Song, Y. Pore structure evolution of organic-rich shale induced by structural deformation based on shale deformation experiments. *Energy*, 2024, **306**, 132463. https://doi.org/10.1016/j.energy.2024.132463
5. Jiang, X., Chen, M., Li, Q., Liang, L., Zhong, Z., Yu, B. et al. Study on the feasibility of the heat treatment after shale gas reservoir hydration fracturing. *Energy*, 2022, **254**, 124422. https://doi.org/10.1016/j.energy.2022.124422
6. Hu, S., Zhao, W., Hou, L., Yang, Z., Zhu, R., Wu, S. et al. Development potential and technical strategy of continental shale oil in China. *Petroleum Exploration and Development*, 2020, **47**(4), 877–887. https://doi.org/10.1016/S1876-3804(20)60103-3
7. Hu, L., Zhu, Y., Chen, S., Du, Z. Fractal characteristics of pore structure of shale in Shuanghe Longmaxi Formation, southern Sichuan Basin. *Xinjiang Petroleum Geology*, 2013, **34**(1), 79–82.
8. Sun, L., Liu, H., He, W., Li, G., Zhang, S., Zhu, R. et al. An analysis of major scientific problems and research paths of Gulong shale oil in Daqing Oilfield, NE China. *Petroleum Exploration and Development*, 2021, **48**(3), 527–540. https://doi.org/10.1016/S1876-3804(21)60043-5
9. Geng, Y., Liang, W., Liu, J., Cao, M., Kang, Z. Evolution of pore and fracture structure of oil shale under high temperature and high pressure. *Energy & Fuels*, 2017, **31**(10), 10404–10413. https://doi.org/10.1021/acs.energyfuels.7b01071
10. Liu, Z., Meng, Q., Dong, Q., Zhu, J., Guo, W., Ye, S. et al. Characteristics and resource potential of oil shale in China. *Oil Shale*, 2017, **34**(1), 15–41. https://doi.org/10.3176/oil.2017.1.02
11. Atchley, S. C., Crass, B. T., Prince, K. C. The prediction of organic-rich reservoir facies within the Late Pennsylvanian Cline shale (also known as Wolfcamp D), Midland Basin, Texas. *AAPG Bulletin*, 2021, **105**(1), 29–52. https://doi.org/10.1306/07272020010
12. Zheng, X., Zhang, B., Sanei, H., Bao, H., Meng, Z., Wang, C. et al. Pore structure characteristics and its effect on shale gas adsorption and desorption behavior.

Marine and Petroleum Geology, 2019, **100**, 165–178. https://doi.org/10.1016/j.marpetgeo.2018.10.045

13. Cheng, G., Wu, C., Jiang, B., Li, F., Li, M., Song, Y. Pore structure evolution of organic-rich shale induced by structural deformation based on shale deformation experiments. *Energy*, 2024, **306**, 132463. https://doi.org/10.1016/j.energy.2024.132463
14. Wang, Q., Hu, Q., Zhao, C., Zhang, C., Ilavsky, J., Yu, L. et al. Integrated experimental studies of pore structure and fluid uptake in the Bossier Shale in eastern Texas, USA. *Fuel*, 2025, **384**, 133926. https://doi.org/10.1016/j.fuel.2024.133926
15. Chen, S., Gong, Z., Li, X., Wang, H., Wang, Y., Zhang, Y. Pore structure and heterogeneity of shale gas reservoirs and its effect on gas storage capacity in the Qiongzhusi Formation. *Geoscience Frontiers*, 2021, **12**(6), 101244. https://doi.org/10.1016/j.gsf.2021.101244
16. Wang, X., Hou, J., Li, S., Dou, L., Song, S., Kang, Q. et al. Insight into the nanoscale pore structure of organic-rich shales in the Bakken Formation, USA. *Journal of Petroleum Science and Engineering*, 2020, **191**, 107182. https://doi.org/10.1016/j.petrol.2020.107182
17. Chen, X., Tang, X., Liu, C., Zhou, X., Guo, S., Yin, H. Implications of temperature for the modification of high-overmature shale reservoirs: experimental and numerical analysis. *SPE Journal*, 2024, **29**(08), 4218–4231. https://doi.org/10.2118/219762-PA
18. Hu, D., Wei, Z., Liu, R., Wei, X., Chen, F., Liu, Z. Enrichment control factors and exploration potential of lacustrine shale oil and gas: a case study of Jurassic in the Fuling area of the Sichuan Basin. *Natural Gas Industry B*, 2022, **9**(1), 1–8. https://doi.org/10.1016/j.ngib.2021.08.012
19. Hu, D., Wei, Z., Liu, R., Wei, X., Liu, Z., Chen, F. Major breakthrough of shale oil and gas in Well Taiye 1 in Bashansi Syncline in the Sichuan Basin and its significance. *China Petroleum Exploration*, 2021, **26**(2), 21–32. https://doi.org/10.3969/j.issn.1672-7703.2021.02.003
20. Fang, R., Jiang, Y., Sun, S., Luo, Y., Qi, L., Dong, D. et al. Controlling factors of organic matter accumulation and lacustrine shale distribution in Lianggaoshan Formation, Sichuan Basin, SW China. *Frontiers in Earth Science*, 2023, **11**, 1218215. https://doi.org/10.3389/feart.2023.1218215
21. Bai, X., Wang, X., Wang, M., Li, J., Lu, S., Yang, X. et al. Occurrence characteristics and factors that influence shale oil in the Jurassic Lianggaoshan Formation, northeastern Sichuan Basin. *Marine and Petroleum Geology*, 2025, **171**, 107197. https://doi.org/10.1016/j.marpetgeo.2024.107197
22. Wang, X., Wang, M., Zhao, C., Yang, X., Jia, Y., Wu, R. et al. Reservoir characteristics and controlling factors of the middle–high maturity multiple lithofacies reservoirs of the Lianggaoshan Formation shale strata in the northeastern Sichuan basin, China. *Marine and Petroleum Geology*, 2024, **161**, 106692. https://doi.org/10.1016/j.marpetgeo.2024.106692
23. He, W., He, H., Wang, Y., Cui, B., Meng, Q., Guo, X. et al. Major breakthrough

and significance of shale oil of the Jurassic Lianggaoshan Formation in Well Ping'an 1 in northeastern Sichuan Basin. *China Petroleum Exploration*, 2022, **27**(1), 40–49. https://doi.org/10.3969/j.issn.1672-7703.2022.01.004

24. Chen, S., Gao, X., Wang, L., Lu, J., Liu, C., Tang, H. et al. Factors controlling oiliness of Jurassic Lianggaoshan tight sands in central Sichuan Basin, SW China. *Petroleum Exploration and Development*, 2014, **41**(4), 468–474. https://doi.org/10.1016/S1876-3804(14)60053-7
25. Kane, O. I., Hu, M., Cai, Q., Deng, Q., Yang, W., Zuo, M. Sedimentary facies, lithofacies paleogeography, and an evaluation of the Ordovician sequences in the Sichuan Basin, southwest China. *Marine and Petroleum Geology*, 2023, **149**, 106096. https://doi.org/10.1016/j.marpetgeo.2023.106096
26. He, W., Bai, X., Meng, Q., Li, J., Zhang, D., Wang, Y. Accumulation geological characteristics and major discoveries of lacustrine shale oil in Sichuan Basin. *Acta Petrolei Sinica*, 2022, **43**(7), 885–898. https://doi.org/10.7623/syxb202207001
27. Schlanser, K., Grana, D., Campbell-Stone, E. Lithofacies classification in the Marcellus Shale by applying a statistical clustering algorithm to petrophysical and elastic well logs. *Interpretation*, 2016, **4**(2), 31–49. https://doi.org/10.1190/INT-2015-0128.1
28. Bhattacharya, S., Carr, T. R., Pal, M. Comparison of supervised and unsupervised approaches for mudstone lithofacies classification: case studies from the Bakken and Mahantango-Marcellus Shale, USA. *Journal of Natural Gas Science and Engineering*, 2016, **33**, 1119–1133. https://doi.org/10.1016/j.jngse.2016.04.055
29. Wang, D., Chen, C., Liu, Z., Yang, S., Liu, M., Xie, J. Main controlling factors for oil and gas enrichment in Jurassic laminated shale in Fuxing area of Sichuan Basin. *Petroleum Geology & Experimentation*, 2024, **46**(2), 319–332. https://doi.org/10.11781/sysydz202402319
30. Cheng, D., Zhang, Z., Hong, H., Zhang, S., Qin, C., Yuan, X. et al. Sequence structure, sedimentary evolution and their controlling factors of the Jurassic Lianggaoshan Formation in the East Sichuan Basin, SW China. *Petroleum Exploration and Development*, 2023, **50**(2), 293–305. https://doi.org/10.1016/S1876-3804(23)60388-X
31. Wang, Y., Zhou, S., Liang, F., Huang, Z., Li, W., Yan, W. et al. Reservoir space characterization of Ordovician Wulalike Formation in northwestern Ordos Basin, China. *Processes*, 2023, **11**(9), 2791. https://doi.org/10.3390/pr11092791
32. Zhou, X., Zhao, Z. Digital evaluation of nanoscale-pore shale fractal dimension with microstructural insights into shale permeability. *Journal of Natural Gas Science and Engineering*, 2020, **75**, 103137. https://doi.org/10.1016/j.jngse.2019.103137
33. Yan, H., Zhou, T., Zhou, X., Liu, X., Tang, X. Non-monotonic evolution and spatial reorganization mechanism of thermally induced micro-damage in sandstone. *Advances in Geo-Energy Research*, 2025, **17**(2), 135–148. https://doi.org/10.46690/ager.2025.08.05
34. IUPAC, I.U.O.P. Physical Chemistry Division Commission on Colloid and Surface Chemistry, Subcommittee on Characterization of Porous Solids:

Recommendations for the characterization of porous solids (technical report). *Pure and Applied Chemistry*, 1994, **66**(8), 1739–1758.

35. Pan, Y., Ji, B., Zhang, W., Knott, K., Xia, Y., Li, Q. et al. Topography and structural regulation-induced enhanced recovery of lithium from shale gas produced water via polyethylene glycol functionalized layered double hydroxide. *Journal of Industrial and Engineering Chemistry*, 2025, **145**, 372–383. https://doi.org/10.1016/j.jiec.2024.10.032
36. Wang, J., Zhang, P., Lu, S., Lin, Z., Li, W., Zhang, J. et al. Insights into microscopic oil occurrence characteristics in shales from the Paleogene Funing Formation in Subei Basin, China. *Petroleum Science*, 2025, **22**(1), 55–75. https://doi.org/10.1016/j.petsci.2024.07.025
37. Su, S., Cheng, C., Jiang, Z., Shan, X., Makeen, Y. M., Gao, Z. et al. Microscopic pore structure and connectivity of lacustrine shale of the Shahejie Formation, Zhanhua Sag, Bohai Bay Basin. *Geoenergy Science and Engineering*, 2023, **226**, 211800. https://doi.org/10.1016/j.geoen.2023.211800
38. Xu, Q., Liu, B., Ma, Y., Song, X., Wang, Y., Chen, Z. Geological and geochemical characterization of lacustrine shale: a case study of the Jurassic Da'anzhai member shale in the central Sichuan Basin, southwest China. *Journal of Natural Gas Science and Engineering*, 2017, **47**, 124–139. https://doi.org/10.1016/j.jngse.2017.09.008
39. Loucks, R. G., Ruppel, S. C., Wang, X., Ko, L., Peng, S., Zhang, T. et al. Pore types, pore-network analysis, and pore quantification of the lacustrine shale-hydrocarbon system in the Late Triassic Yanchang Formation in the southeastern Ordos Basin, China. *Interpretation*, 2017, **5**(2), 63–79. https://doi.org/10.1190/INT-2016-0094.1
40. Liang, F., Zhang, Q., Lu, B., Chen, P., Su, C., Zhang, Y. et al. Pore structure in shale tested by low pressure N_2 adsorption experiments: mechanism, geological control and application. *Energies*, 2022, **15**(13), 4875. https://doi.org/10.3390/en15134875
41. Medina-Rodriguez, B. X., Alvarado, V. Use of gas adsorption and inversion methods for shale pore structure characterization. *Energies*, 2021, **14**(10), 2880. https://doi.org/10.3390/en14102880
42. Mostefai, R., Kadri, M. M., Senoussi, E., Hacini, M., Awadh, S. M. Pore structure characterization of shale reservoir using nitrogen adsorption-desorption. *Iraqi Geological Journal*, 2023, **56**(1D), 1–13. https://doi.org/10.46717/igj.56.1D.1ms-2023-4-10
43. Spacapan, J. B., Ruiz, R., Manceda, R., D'Odorico, A., Rocha, E., Vera, E. R. et al. Oil production from a sill complex within the Vaca Muerta Formation. In *Integrated Geology of Unconventionals: The Case of the Vaca Muerta Play, Argentina* (Minisini, D., Fantín, M., Noguera, I. L., Leanza, H. A., eds). AAPG Memoir 121, 2020, Tulsa.
44. Gale, J. F. W., Fall, A., Yurchenko, I. A., Ali, W. A., Laubach, S. E., Eichhubl, P. et al. Opening-mode fracturing and cementation during hydrocarbon generation in shale: an example from the Barnett Shale, Delaware Basin, West Texas. *AAPG Bulletin*, 2022, **106**(10), 2103–2141. https://doi.org/10.1306/01062219274

45. Iltaf, K. H., Hu, Q., Fan, M., Oware, P., Wang, Q., Zhao, C. et al. Multiscale pore characterization of the New Albany Shale: insights from complementary analytical techniques. *Energy & Fuels*, 2025, **39**(22), 10356–10373. https://doi.org/10.1021/acs.energyfuels.5c00862
46. Garum, M., Glover, P. W. J., Lorinczi, P., Micklethwaite, S., Hassanpour, A. Integration of multiscale imaging of nanoscale pore microstructures in gas shales. *Energy & Fuels*, 2021, **35**(13), 10721–10732. https://doi.org/10.1021/acs.energyfuels.1c00554
47. Ruppert, L. F., Jubb, A. M., Headen, T. F., Youngs, T. G. A., Bandli, B. Impacts of mineralogical variation on CO_2 behavior in small pores from producing intervals of the Marcellus Shale: results from neutron scattering. *Energy & Fuels*, 2020, **34**(3), 2765–2771. https://doi.org/10.1021/acs.energyfuels.9b03744
48. Garum, M., Glover, P. W. J., Lorinczi, P., Drummond-Brydson, R., Hassanpour, A. Micro-and nano-scale pore structure in gas shale using Xμ-CT and FIB-SEM techniques. *Energy & Fuels*, 2020, **34**(10), 12340–12353. https://doi.org/10.1021/acs.energyfuels.0c02025
49. Fatah, A., Mahmud, H. B., Bennour, Z., Gholami, R., Hossain, M. The impact of supercritical CO_2 on the pore structure and storage capacity of shales. *Journal of Natural Gas Science and Engineering*, 2022, **98**, 104394. https://doi.org/10.1016/j.jngse.2021.104394
50. Sun, Y., Wang, Y., Liu, J., Wang, Y. A pyrolysis study of kerogen and extracted bitumen from a lacustrine shale of the Shahejie Formation and implications for in-situ conversion processes. *Journal of Analytical and Applied Pyrolysis*, 2024, **183**, 106735. https://doi.org/10.1016/j.jaap.2024.106735
51. Shi, S., Wang, Y., Chen, C., Liu, J., Peng, P. Influence of tectonic evolution processes on burial, thermal maturation and gas generation histories of the Wufeng-Longmaxi shale in the Sichuan Basin and adjacent areas. *International Journal of Coal Geology*, 2024, **295**, 104642. https://doi.org/10.1016/j.coal.2024.104642
52. Slatt, R. M., O'Brien, N. R. Pore types in the Barnett and Woodford gas shales: contribution to understanding gas storage and migration pathways in fine-grained rocks. *AAPG Bulletin*, 2011, **95**(12), 2017–2030. https://doi.org/10.1306/03301110145
53. Pfeifer, P., Avnir, D. Chemistry in noninteger dimensions between two and three. I. Fractal theory of heterogeneous surfaces. *The Journal of Chemical Physics*, 1983, **79**(7), 3558–3565. https://doi.org/10.1063/1.446210
54. Li, K., Zeng, F., Cai, J., Sheng, G., Xia, P., Zhang, K. Fractal characteristics of pores in Taiyuan formation shale from Hedong coal field, China. *Fractals*, 2018, **26**(02), 1840006. https://doi.org/10.1142/S0218348X18400066
55. Yang, F., Ning, Z., Liu, H. Fractal characteristics of shales from a shale gas reservoir in the Sichuan Basin, China. *Fuel*, 2014, **115**, 378–384. https://doi.org/10.1016/j.fuel.2013.07.040